Atomic Hydrogen and Star Formation in the Bridge/Ring Interacting Galaxy Pair NGC 7714/7715 (Arp 284)

Beverly J. Smith IPAC/Caltech, MS 100-22, Pasadena CA 91125

Curtis Struck

Department of Physics and Astronomy, Iowa State University, Ames IA 50012 and

Richard W. Pogge

Department of Astronomy, Ohio State University, 174 W. 18th Ave, Columbus OH 43210

To be	e published	in the	July 10	, 1997	issue	of the	${\bf Astrophysical}$	Journal
1	Danimad]	

ABSTRACT

We present high spatial resolution 21 cm HI maps of the interacting galaxy pair NGC 7714/7715. We detect a massive $(2 \times 10^9 \mathrm{M}_{\odot})$ HI bridge connecting the galaxies that is parallel to but offset from the stellar bridge. A chain of HII regions traces the gaseous bridge, with $H\alpha$ peaks near but not on the HI maxima. An HI tidal tail is also detected to the east of the smaller galaxy NGC 7715, similarly offset from a stellar tail. The strong partial stellar ring on the east side of NGC 7714 has no HI counterpart, but on the opposite side of NGC 7714 there is a $10^9 \mathrm{M}_{\odot}$ HI loop ~ 11 kpc in radius. Within the NGC 7714 disk, clumpy HI gas is observed associated with star formation regions. Redshifted HI absorption is detected towards the strong starburst nucleus. We compare the observed morphology and gas kinematics with gas dynamical models in which a low-mass companion has an off-center prograde collision with the outer disk of a larger galaxy. These simulations suggest that the bridge in NGC 7714/7715 is a hybrid between the tidal bridges seen in systems like M51 and the purely gaseous 'splash' bridges found in ring galaxies like the Cartwheel. The offset between the stars and gas in the bridge may be due to dissipative cloud-cloud collisions occurring during the impact of the two gaseous disks.

Subject headings: galaxies: individual (NGC 7714/7715) - galaxies: interactions - galaxies: kinematics and dynamics - radio lines: atomic

1. Introduction

It is well-established that gravitational encounters between galaxies can create tidal tails and bridges (Toomre & Toomre 1972; Wright 1972). It is also well-known that head-on collisions between unequal mass galaxies can create rings (Lynds & Toomre 1976; Theys & Spiegel 1977). Luminous HII regions have been observed in extended tidal features (Schweizer 1978; Mirabel et al. 1991, 1992; Hibbard & van Gorkom 1996) as well as in collisional rings (Fosbury & Hawarden 1977; Higdon 1995; Marston & Appleton 1995), indicating that interactions can trigger star formation in these peculiar structures.

A particularly interesting class of interacting galaxies are those pairs containing both a bridge and a collisional ring. The location of the bridge in a bridge/ring system may indicate which of multiple companions collided with the ring galaxy, as in the Cartwheel galaxy (Higdon 1996) and in VII Zw 466 (Appleton et al. 1996), while the composition of the bridge may provide clues to how it formed. Two different mechanisms are capable of creating bridges between galaxies. As discussed by Toomre & Toomre (1972), tidal forces and spin-orbit coupling during an encounter are capable of drawing both gas and stars out into a bridge. A well-known example of a tidal bridge is found in the M51 system (Toomre & Toomre 1972). Tidal bridges have been modeled in detail by Barnes & Hernquist (1991) and Mihos & Hernquist (1996) using a hybrid N-body/hydrodynamical code. In these simulations, the impact parameters used are greater than the disk radii, so an immediate collision between the two galaxies does not occur. The second type of bridge, a 'splash' bridge, is the result of a purely hydrodynamical effect and occurs during smaller impact parameter encounters (Appleton et al. 1996; Struck 1996a, 1996b). In this version of the standard ring galaxy model, both galaxies initially contain gaseous disks. During the passage of the smaller galaxy through the larger disk, gas clouds from the two galaxies collide, creating a bridge between the two galaxies. In this class of bridge formation models, a stellar counterpart to the gaseous bridge is not formed and the expected gas surface density in the bridge is relatively low (Struck 1996a). The HI bridges seen in the Cartwheel (Higdon 1996) and VII Zw 466 systems (Appleton et al. 1996) may be this type of bridge, rather than tidal bridges (Struck 1996a; Struck et al. 1996), because the observed bridges are purely gaseous.

In this paper, we present new 21 cm HI and narrowband optical images of the bridge/ring system NGC 7714/7715 (Arp 284), and discuss them in the context of ring and bridge formation models. This system differs dramatically from the Cartwheel and VII Zw 466 systems in having a prominent stellar bridge as well as only a partial ring (Arp 1966). In addition, NGC 7714 differs from the other two galaxies by having tidal tails (Arp 1966) and a strong bar (Bushouse & Werner 1990). This complex morphology may have been caused by a more off-center encounter than that which produced the more symmetric rings in the Cartwheel and VII Zw 466. In Smith & Wallin (1992; hereafter Paper I), we used a restricted 3-body model to simulate the NGC 7714/7715 encounter, and successfully reproduced the observed optical structure with an off-center (impact parameter $r_{min} \sim 0.85$ times the radius of the larger disk) inclined collision between two unequal-mass disk galaxies $(M_2/M_1 \sim 0.3)$. NGC 7714/7715 is somewhat reminiscent of the 'Sacred Mushroom' galaxy AM 1724-622 (Arp & Madore 1986), which also contains a ring and a stellar bridge. AM 1724-622, however, does not have tidal tails and therefore may have undergone a less off-center ($r_{min} \sim 0.5 r_{disk}$) collision than NGC 7714/7715 (Wallin & Struck-Marcell 1994).

The distribution of star formation in NGC 7714 also differs from that in many ring galaxies. In contrast to the outer ring in the Cartwheel (Fosbury & Hawarden 1977; Higdon 1995) and the ring galaxies surveyed by Marston & Appleton (1995), the NGC 7714 ring does not have on-going star formation (Bushouse & Werner 1990; Bernlöhr 1993; González-Delgado et al. 1995). The near-infrared colors of the NGC 7714 ring imply a

considerable older stellar component (Bushouse & Werner 1990), while the Cartwheel's outer ring is primarily composed of young stars (Marcum, Appleton, & Higdon 1992; Higdon 1995). The NGC 7714 ring resembles the inner ring of the Cartwheel, which has an older stellar population (Marcum et al. 1992) and little star formation (Higdon 1995), as well as the ring in AM 1724-622, which is also composed of mainly older stars (Wallin & Struck-Marcell 1994).

Star formation in NGC 7714 is occurring at the nucleus, near the northern end of the bar, and at the base of the southwestern tidal tail instead of in the ring (Bushouse & Werner 1990; Bernlöhr 1993; González-Delgado et al. 1995). The luminous starburst nucleus in this galaxy is well-studied (French 1980; Weedman et al. 1981; Keel 1984; de Robertis & Shaw 1988) and is known to contain Wolf-Rayet stars (van Breugel et al. 1985; González-Delgado et al. 1995). Luminous HII regions are also seen in the bridge between the two galaxies but not in the companion NGC 7715 (Arp 1966; Bernlöhr 1993; González-Delgado et al. 1995). NGC 7715 has no optical emission lines (Humanson, Mayall, & Sandage 1956; Bernlöhr 1993); spectral synthesis indicates that it is in a post-starburst stage, with a large population of A and late-type B stars (Bernlöhr 1993). Most of the far-infrared emission from this system arises from NGC 7714 (Surace et al. 1993).

In our previous study of this system (Paper I), we presented low resolution (40") 21 cm HI maps obtained with the NRAO Very Large Array (VLA¹) in the D array configuration. These observations showed that the atomic hydrogen in this system is very extended, reaching out to a maximum radius of 6' (\sim 70 kpc). Between the two galaxies, a gaseous bridge is seen. In spite of its high star formation rate, NGC 7714 is relatively weak in the standard tracer of molecular gas, the millimeter CO (1 – 0) line (Sanders, Scoville, & Soifer 1991; Young & Devereux 1991). The M_{H_2}/M_{HI} ratio in the inner 45" has the unusually low

¹The VLA is operated by Associated Universities, Inc., under contract with the NSF.

value of 0.75, assuming the standard Galactic I_{CO}/N_{H_2} ratio (Paper I). This may be due to the low metallicity of this system (Weedman et al. 1991; González-Delgado et al. 1995) rather than a true deficiency of molecular gas (Paper I). Interferometric observations show that the CO peak in NGC 7714 is a few arcseconds north of the optical and radio continuum nucleus, and is extended about 10" east-west with a spur extending south towards the nucleus (Ishizuki 1993).

The VLA and optical observations of NGC 7714/7715 are described in Section 2 of this paper, while the data are described in Section 3. To better understand the role of tidal and hydrodynamical effects in shaping the gas morphology of this system, in Section 4 we present a hydrodynamical model of a low mass disk galaxy impacting the outer disk of a larger galaxy. Implications of the observations and model are discussed in Section 5, and conclusions given in Section 6. Table 1 provides some basic information about the two galaxies in this system. A distance to these galaxies of 37 Mpc is assumed throughout this paper ($H_o = 75 \text{ km s}^{-1} \text{ Mpc}^{-1}$).

2. Observations and Data Reduction

2.1. Very Large Array

The new HI data were obtained with the B and C array configurations of the VLA. The C Array observations were made on 1992 May 21, while the B Array measurements were obtained on 1994 July 10. The total integration time on NGC 7714/7715 was 8 hours with the C Array and 7.5 hours with the B Array. During both observing runs, 3C 286 and 3C 48 were each observed for 20 minutes for flux and bandpass calibration, and a nearby phase calibrator was observed every 30 minutes for 5 minutes. On-line Hanning smoothing was used for the observations, giving 63 channels with a resolution of 10.5 km s⁻¹ and a

total bandwidth of 655 km $\rm s^{-1}$ centered at 2800 km $\rm s^{-1}$.

Calibration and mapping were accomplished using the NRAO Astronomical Image Processing System (AIPS). After calibration, the first step in the data reduction was to make a continuum map from 21 line-free channels near the ends of the bandpass. This map was then CLEANed (Clark 1980) and the CLEAN components were subtracted from the original UV database. A set of continuum-free maps were then constructed and residual continuum emission removed. The maps were then CLEANed to remove sidelobes due to the HI emission. Finally, a correction for primary beam attenuation was made. To obtain the highest sensitivity possible, natural weighting was used for these maps. A set of maps was obtained from the B Array data alone, giving a final beamsize of $6''.32 \times 5''.79$ with a position angle of 2.7 and a noise level of 0.39 mJy beam⁻¹ channel⁻¹. A second set of maps was made after combining the B and C Array data with the D Array data from Paper I. The final beamsize for the B+C+D Array dataset is $11''.02 \times 8''.48$ with a position angle of -36.6 and noise level of 0.32 mJy beam⁻¹ channel⁻¹. The B Array datacube was made with 1024×1024 pixels and 1" pixel⁻¹, while the B+C+D Array maps have 512×512 pixels with 2" pixel⁻¹. The final B+C+D Array HI channel maps are shown in Figure 1. Emission is seen in 25 channels, from 2674 km s^{-1} to 2926 km s^{-1} .

HI intensity maps were made from these two sets of channel maps using the AIPS moment routines. To determine which pixels from the cube should be excluded in constructing the final B Array intensity map, a scratch copy of the datacube was Hanning smoothed to 31.2 km s⁻¹ and convolved with a $7'' \times 7''$ FWHM Gaussian beam. Only pixels above 0.65 mJy beam⁻¹ in this smoothed cube were included in deriving the final map from the original unsmoothed cube. To search for more extended emission, the same method was used on the higher sensitivity B+C+D Array datacube to construct a second HI intensity map. For this second map, the scratch cube was Hanning smoothed to 31.2 km

s⁻¹ and convolved with a $16'' \times 16''$ Gaussian beam. Data below $0.85 \text{ mJy beam}^{-1}$ in the smoothed cube were excluded in making the moment 0 map. We also construct a moment 1 HI velocity map from the B+C+D Array dataset. In deriving this map, we use a scratch cube smoothed with a $16'' \times 16''$ FWHM Gaussian and a $1.1 \text{ mJy beam}^{-1}$ flux cutoff, with no velocity smoothing.

2.2. Narrowband Optical Imaging

NGC 7714/7715 was observed on the night of 1991 October 8 with the 1.8m Perkins Telescope of the Ohio State and Ohio Wesleyan Universities at Lowell Observatory. The Ohio State University Imaging Fabry-Perot Spectrograph was used in its direct imaging mode with the Lowell NSF TI 800 × 800 CCD detector. This setup gives 0.49'' pixel⁻¹. Two 50 \mathring{A} interference filters at 6660 \mathring{A} and 6560 \mathring{A} were used to produce on- and off-H α images, respectively. The total exposure time per filter was 1800 sec. The seeing was 1".7.

The images were flat-field and de-biased in a standard fashion, and then registered, scaled, and subtracted to produce a pure emission-line image. Final registration was accomplished using stellar positions measured by the McDonald Observatory PDS machine, as in Paper I. Since this image was obtained during nonphotometric conditions, it was approximately flux calibrated using the total H α flux of the system from González-Delgado et al. (1995).

3. Observational Results

3.1. The Narrowband Optical Images

The final narrowband continuum and H α images are shown in Figures 2a and 2b, respectively. Figure 2b is consistent with previous H α maps of the system (Bushouse & Werner 1990; Bernlöhr 1993; González-Delgado et al. 1995). Massive star formation is observed in the nucleus of NGC 7714; this nuclear HII region complex is asymmetric, with an eastern extension. Luminous HII regions lie along an arc at the northern end of the NGC 7714 bar and at the base of the southwestern tail, but no H α emission is detected from the NGC 7714 ring. A prominent chain of HII regions is visible in the bridge connecting the two galaxies. No HII regions are seen in NGC 7715. In the optical continuum image (Figure 2a), both galaxies are seen, and the NGC 7714 ring and bar are visible.

3.2. The Radio Continuum Map

The B Array continuum map is shown in Figure 3. The center of NGC 7714 and a triple source to the northeast of NGC 7715 (a background object) are seen in this plot; NGC 7715 is not detected in the radio continuum. NGC 7714 has a bright central core surrounded by diffuse extended emission. The peak and total 20 cm B Array continuum flux density for NGC 7714 are 26 mJy beam⁻¹ and 77 mJy, compared to 59 mJy beam⁻¹ and 71 mJy, respectively, for the D Array data (Paper I). The HII region complex at the base of the southwestern tail of NGC 7714 is resolved in this map. It has a total 20 cm continuum flux of 3.5 mJy.

The positions and peak flux densities of the three peaks in the background source are tabulated in Table 2. Source #2 is coincident with the z=1.87 18th magnitude optical quasar 2333+0154 (Bowen et al. 1994). The double-lobed radio structure of this object was previously noted by Neff, Hutchings, & Gower (1989). The total B Array flux density for

this background object is 176 mJy, compared to 157 mJy from the D Array (Paper I).

3.3. The HI Intensity Maps

In Figure 4a, we present the naturally-weighted B Array HI intensity map, while in Figure 4b, the naturally-weighted B+C+D Array HI intensity map is given. Figures 5a and 5b show an expanded view of the higher resolution B Array HI intensity map superposed on the narrow band optical continuum image and the H α image, respectively. To search for low level optical continuum emission, we have smoothed the red Digitized Sky Survey² data for this region to 12" resolution. It is overlaid on the B+C+D Array HI intensity map in Figure 6.

The HI morphology of this system is very disturbed and the gas extends well beyond the main optical disks of the galaxies. Particularly prominent in these maps is an HI bridge between the two galaxies. This bridge is offset $\sim 10''$ (1.8 kpc) to the north of the optical bridge (Figure 6). The H α sources apparent in the bridge lie near, but not on, the HI peaks (Figure 5b). Massive star formation is occurring in the gaseous bridge rather than in the more southern stellar bridge. This effect is also seen in the Arp Atlas (Arp 1966) photograph of NGC 7714; the H II regions lie to the north of the smoother stellar bridge.

Tidal HI is seen in other locations as well. Strong HI is observed in a prominent countertail to the east of NGC 7715. This feature is hereafter named the 'eastern cloud'.

²The Digitized Sky Survey, a compressed digital form of the Palomar Observatory Sky Atlas, was produced at the Space Telescope Science Institute under U.S. Government grant NAG W-2166. The National Geographic Society - Palomar Observatory Sky Atlas (POSS-I) was made by the California Institute of Technology with grants from the National Geographic Society.

HI is relatively weak at NGC 7715; in the less sensitive B Array data a gap is observed between the eastern cloud and the bridge. In the higher sensitivity B+C+D Array data this gap is filled in with more diffuse gas. As at the bridge, the gas appears skewed to the north relative to the optical light throughout both NGC 7715 and the eastern tail.

On the other side of the system, there is a bright arc or loop of HI 1' northwest of NGC 7714 (the 'northwestern loop'). The smoothed POSS image (Figure 6) shows a possible optical counterpart to this HI loop. Finally, to the far west, there are numerous HI clouds that extend several arcminutes from the center of NGC 7714 (Figure 4b).

Our data also provide a closer look at NGC 7714 itself. Figures 4a and 4b show an apparent HI hole at the optical nucleus of NGC 7714; this depression may be due to HI absorption (see Section 3.5). In the disk of NGC 7714, the HI is not confined to a bar or to an HI ring tracing the optical ring (Figure 5a). Instead, the gas is quite clumpy, with two HI holes at the outer edge of the stellar ring and another depression near the southern end of the bar (Figure 5a). South of the ring there is an arc of gas extending to the southeast (the 'southeastern arc'). Particularly large clumps of gas are seen near the star formation regions northwest and southwest of the nucleus (the 'northwestern' and 'southwestern clumps'). The southwestern clump lies at the base of the optical tail. In these regions, the H α peaks are close to but not coincident with the HI peaks. There is also an HI peak inside the ring (Figure 5a). There is a small HII region outside of this HI clump, on the inner edge of the ring (Figure 5b). This clump of gas may be foreground or background bridge material rather than disk gas, and may not lie in the same plane as the ring. Its presence therefore complicates the search for a gaseous counterpart to the ring.

We find a total HI flux for this system of $21.8 \text{ Jy km s}^{-1}$, comparable to the 10' aperture single dish measurements of $17.9 \text{ Jy km s}^{-1}$ (Peterson & Shostak 1974) and $21.0 \text{ Jy km s}^{-1}$ (Bushouse 1987). The HI masses and peak column densities of the various

structures are given in Table 3. More than half of the total atomic gas in the system lies outside of the optical disks. The HI masses of the bridge and the western loop are especially large, greater than 10^9 M_{\odot} . The peak HI column density in the bridge, $5.4 \times 10^{21} \text{ cm}^{-2}$ in a 6" beam, is particularly high.

3.4. The HI Velocity Structure

In Figure 7, the HI velocity profiles for various structures in the NGC 7714/7715 system are shown. The peak velocities and FWHM line widths of these features are included in Table 3. The total profile agrees with the single dish observations of Peterson & Shostak (1974). The gas in the bridge and eastern cloud is quite confined in velocity, as is typical of tidal features, while the western loop has a relatively broad velocity profile. The profiles for the individual clumps in the NGC 7714 disk are relatively narrow.

In Figures 8a and 8b, we plot the HI velocity field with the narrowband optical continuum map and the B+C+D Array HI intensity map, respectively. East to west across the system from the eastern cloud through the bridge, a shallow velocity gradient of 3.5 km s⁻¹ kpc⁻¹ is observed, with the gas in the eastern cloud being more blueshifted. At NGC 7715 the gas is more redshifted than expected by this trend (Figure 8a). Across the optical body of NGC 7715, the velocity field suggests rotation with a line of nodes parallel to the major axis of the galaxy and the western side redshifted (Figure 8a). A velocity change of 50 km s⁻¹ is observed over 20" (3.6 kpc), and the systemic velocity is 2800 km s⁻¹, equal to that of NGC 7714. Thus the kinematics of the gas in the immediate vicinity of NGC 7715 appear distinct from those of the surrounding extended gas.

In the disk of NGC 7714, the velocity field indicates the presence of an inclined rotating disk of gas, with more redshifted gas to the northwest. The line of nodes is approximately

parallel to the bar, at a position angle of $\sim 132^\circ$ in the inner disk, decreasing slightly with increasing radius. The velocity field shows maxima and minima beyond the end of the bar at radii of 15'' - 20'', suggesting that the rotation curve turns over at that radius. Relative to the systemic velocity, the maximum rotational velocity uncorrected for inclination is 60 km s⁻¹.

The most redshifted gas in the system is in the northwestern loop. East to west along this loop the velocities increase until the point at which the loop bends southward. After that location the gas becomes increasingly blueshifted as the loop arcs southward and connects back to the main galaxy. The position of maximum redshift does not lie along the line of nodes defined by the inner disk, but instead is rotated 20° to the southwest. In the far western HI clouds, the velocity gradient is such that the most northern gas is more redshifted than that in the south.

In Figures 8a and 8b, significant deviations from circular motion are observed. Note the particularly strong peculiar motions at the location of the gaseous bridge (Figure 8b). Figure 8a also shows some curvature in the isovelocity contours at the stellar ring. In addition, there are deviations near the southwestern HI clump, where the gas is more redshifted than expected (Figure 8b). These deviations may be caused by a combination of non-planar and radial motions. It is probable that the gas in the bridge lies in a different plane than the gas in the disk of NGC 7714, and the disk of NGC 7714 itself may be warped. Second, radial motions may be present along the bridge, in the ring, and along the tails. Because of the uncertain geometry of the system it is difficult to distinguish between these possibilities.

From the HI velocity field, we have derived a rotation curve for the inner disk of NGC 7714 (Figure 9). We used a tilted ring model as in Begeman (1989) and weighted the data by the cosine of the azimuthal angle with maximum weighting along the major

axis. Because of the observed deviations from circular motion, we do not iteratively fit all the required parameters for this curve. Instead, we assume that the dynamical center is coincident with the radio continuum nucleus (Condon et al. 1990; Table 1), the systemic velocity is 2800 km s⁻¹, and the line of nodes is fixed at a position angle of 132° east of north (Figure 8b). We also require the inclination to be fixed at 30°. This inclination may be reasonable for the disk of NGC 7714 itself (Paper I), but may well differ at larger radii as indicated by the observed distortions to the velocity field. Therefore, in Figure 9 we only plot the rotation curve out to a radius of 30″. This curve shows a smooth increase in velocity to a radius of 16″ where it drops off slightly.

3.5. HI Absorption

In Figure 10, we plot the continuum-subtracted HI spectrum for the central position of NGC 7714. A weak absorption line with an optical depth of 0.062 ± 0.016 and a velocity width of 40 km s⁻¹ is apparent at a velocity redshifted 100 km s⁻¹ with respect to the systemic velocity of the galaxy. This redshift suggests that gas is infalling onto the starburst nucleus. Assuming a spin temperature of 100K, we find an absorbing column density N(HI) of $4.7 \pm 1.2 \times 10^{20}$ cm⁻² towards the nucleus. Redshifted HI absorption lines towards nuclear radio continuum sources are not uncommon, and are more often redshifted than blueshifted relative to the systemic velocity of the galaxy (Dickey 1986; van Gorkom et al. 1989; Smith 1994).

No HI absorption is seen towards the background continuum sources.

4. An Off-Center Collision between Two Disk Galaxies

Both the stars and the gas in this system appear to be distributed in a highly nonequilibrium and short-lived manner. Moreover, there are large differences in the distribution of the two components. To understand the dynamical processes that produced these morphologies and to relate this system to other collisional galaxies, detailed comparisons between the data and numerical simulations of galaxy interactions are important. In Paper I, we presented a restricted 3-body model of this interaction which reproduced the stellar structure of this system. To understand the behavior of the gas, however, a more sophisticated numerical model which includes hydrodynamical effects is required. Unfortunately, encounters with interaction parameters appropriate for this system have not yet been investigated with hydrodynamical modeling studies. Previously published hydrodynamical models of interacting galaxies have concentrated on either small impact parameter collisions ($r_{min} < 0.5 r_{disk}$) (Appleton & Struck-Marcell 1987; Struck-Marcell & Appleton 1987; Gerber, Lamb, & Balsara 1992, 1996; Struck-Marcell & Higdon 1993; Hernquist & Weil 1993; Appleton et al. 1996; Struck 1996a, 1996b) or encounters without an initial collision ($r_{min} \ge 1 r_{disk}$) (Barnes & Hernquist 1992; Howard et al. 1993; Mihos & Hernquist 1996), while our previous study of NGC 7714/7715 indicates that an impact parameter between these two ranges is needed (Paper I).

To investigate the behavior of interstellar gas in such an encounter, in this section we present a numerical simulation of an off-center collision between two disk galaxies using a smoothed particle hydrodynamics (SPH) code. This model is not an exact representation of NGC 7714/7715 itself, but rather a more general off-center collision which illustrates some of the effects observed in NGC 7714/7715. We are currently working to produce a more detailed model matched to NGC 7714/7715.

The SPH code used is described in detail by Struck (1996a, 1996b). Earlier versions of

this code were used to model the Cartwheel (Struck-Marcell & Higdon 1993) and VII Zw 466 (Appleton et al. 1996) systems. The large-scale collisional dynamics are simulated with a restricted 3-body approximation, while local self-gravity between neighboring gas particles is included. Simplified treatments of gas heating and cooling are also included. Stars are represented as collisionless gas particles which do not participate in heating or cooling. The gas/star particle ratio is about 3/1 and the stellar disk is half the size of the gaseous disk. The primary galaxy contains 13,600 gas particles, while the companion has 4000.

In this simulation, we used a galaxy mass ratio $M_2/M_1 = 0.3$ and an impact parameter $r_{min} = 0.98 \ r_{stellar \ disk} = 0.5 \ r_{gas \ disk}$. The inclination of the companion's orbit relative to the main disk = 120° and the inclination of the larger disk relative to the plane of the sky = 30°. The initial orientation of the companion is 25° out of the x-z plane (the x-y plane is assumed to be the plane of the sky). As in the Paper I model, the encounter is retrograde with respect to the main galaxy and prograde with respect to the smaller galaxy. In contrast to the models in Struck (1996a, 1996b), for this simulation we used a softened point mass potential rather than a rigid halo.

Our final model is shown in Figure 11. The four panels show different particle sets, all at the same timestep. Figure 11a shows the stellar distribution in the x-y plane, while Figures 11b and 11c show two orthogonal views of the gas distribution, in the x-y and x-z planes. In these figures, the near side of the larger disk is to the left and its rotation is clockwise on the sky, while the lower side of the smaller galaxy is closer, with counterclockwise rotation. Figure 11d shows an expanded x-y view of the bridge, with both stars and gas. The time displayed is 10^8 yrs after the point of closest approach, assuming a mass of about 1.2×10^{10} M_{\odot} contained within the main stellar disk.

Following impact, the stellar morphology of this model developed in a manner very similar to that in the Paper I model. Specifically, a ring and two projecting spiral arms

develop in the primary stellar disk, while stars from the companion form a stellar bridge and a countertail. The gas distribution is qualitatively similar to that of the stars, but with some important differences. The gas arms are longer, as expected for the more extended gas disk. There is also a partial ring of gas in the disk of the main galaxy, which lies somewhat to the outside of the stellar ring. Gas is also found in the bridge between the two galaxies, but, unlike the stars in the bridge, this gas originates in both galaxies. As in the Struck (1996a, 1996b) models, gas has been splashed from both galaxies into the bridge by the collision of the two disks.

By varying the initial orbital, disk, and viewing parameters, we are able to change the position of the stellar bridge relative to the gaseous bridge. In particular, the location of the stellar bridge is determined in part by the initial orientation of the companion galaxy, while the impact position and rotation of the main disk affect the location of the splash bridge. In the model shown, an offset between the centroids of the gas bridge and the stellar bridge is apparent, with the stars shifted to the top of the page relative to the gas. This offset is caused by dissipative collisions between gas clouds during the encounter; the gas from the companion becomes displaced from the stars.

5. Discussion

5.1. The Gas/Star Offset in the Bridge

One of the most striking results of this study is the observation of a very gas-rich bridge connecting NGC 7714 and NGC 7715. In this bridge, the gas and stars are offset by ~ 2 kpc. The HI column density in this bridge ($\sim 5 \times 10^{21}$ cm⁻²) is very high compared to other such features. It is about an order of magnitude higher than that observed in the Cartwheel (Higdon 1996) and VII Zw 466 (Appleton et al. 1996) bridges and in many

tidal tails (e.g., Hibbard et al. 1994; Smith 1994; Hibbard & van Gorkom 1996), but is comparable to the HI column density observed in the bridge of the 'Taffy' galaxies, UGC 12914/5, another possible bridge/ring system (Condon et al. 1993).

The NGC 7714/7715 bridge is clearly not a purely 'splash' bridge, as in the models of Struck (1996a, 1996b), because of the existence of the pronounced stellar bridge. It is also probably not a purely tidal bridge; the presence of a stellar ring in NGC 7714 suggests an impact parameter $< r_{disk}$ and therefore a collision of the two gaseous disks. Our hydrodynamical model of an off-center collision between two disk galaxies (Section 4) produces a connecting bridge with both stars and gas. The bridge gas in this model originated in both galaxies, while the stars came from only the companion. We therefore suggest that the bridge in NGC 7714/7715 is a combination of a tidal bridge and a 'splash' bridge, where the stellar bridge has been drawn out by tidal forces and both tidal and hydrodynamical processes created the gaseous bridge. The observed separation between the gas and stars in the NGC 7714/7715 bridge is produced naturally in such a scenario, because the stars and gas in the bridge did not all originate from the same galaxy and because the cross-section of gas is much larger than the cross-section of stars.

Other alternative explanations for the gas/star shift in the NGC 7714/7715 bridge are less likely. An interaction with an intergalactic medium may cause an offset, however, NGC 7714/7715 is an isolated pair, not in a cluster, so one would not expect significant stripping by intergalactic gas. Gas depletion by star formation on the southern edge of bridge could also create the offset. It is likely, however, that the stars in the stellar bridge predate the interaction and were not formed in situ. This possibility should be tested with broadband optical and near-infrared mapping of the bridge.

Gas/star offsets are not uncommon in tidal features. A gas/star shift is observed along about one quarter of the 3' (80 kpc) long Arp 295 bridge (Hibbard & van Gorkom

1996), and similar offsets between the stars and gas have been seen in the tidal tails of a few interacting systems (Wever et al. 1984; Hibbard & van Gorkom 1996). Although these are not ring galaxies, a similar mechanism may be responsible for the observed offsets in some cases: collisions may occur between clouds from the two galaxies when the approach distance is small enough. In one of the larger impact parameter models of Mihos & Hernquist (1996), a pronounced offset between the stars and gas in the bridge is produced by collisions between clouds on intersecting orbits. In many tails no offset is seen (Hibbard & van Gorkom 1996), so observing such an offset may depend on the geometry of the encounter, the gas content, and the timescale. The NGC 7714/7715 interaction is very favorable for the observation of this effect, because of the relatively small impact parameter $(r_{min} < r_{disk})$ compared to non-colliding interacting pairs.

5.2. Gas Accretion From the Bridge

In both the tidal (Hernquist & Barnes 1991; Mihos & Hernquist 1996) and collisional (Struck 1996a, 1996b) models of bridge formation, accretion from the bridge onto the galaxies is expected. In our HI data, we see deviations from circular motion at the bridge, but, as noted in Section 3.4, because of the uncertain geometry of the system it is unclear whether these deviations imply radial motion or simply non-planar circular motion. The interaction is mainly occurring in the plane of the sky, and it is uncertain whether NGC 7714 or NGC 7715 is closer to us. Therefore, our data are inconclusive on the question of gas accretion onto the galaxies from the bridge.

5.3. The Rings

NGC 7714 has two partial rings: a stellar ring to the east, and a larger gaseous ring to the northwest. As noted previously, these rings differ from those in many ring galaxies in not having on-going star formation. Like the non-star-forming inner ring of the Cartwheel but unlike the Cartwheel's outer ring (Higdon 1996), the optical ring in NGC 7714 does not have a prominent HI counterpart. Instead, HI depressions are observed on the outer edge of the ring and at the southern end of the bar. Our hydrodynamical model of an off-center collision (Section 4) shows that such differentiation of gas and stars is expected in partial rings formed during very off-center collisions. Thus the lack of an HI counterpart does not rule out a collisional origin for the NGC 7714 ring. This point will be investigated further in future modeling studies.

One of the best methods of testing the collisional ring hypothesis is to search for kinks in the velocity field across the rings. In the more symmetrical ring galaxy the Cartwheel, such kinks are observed and are consistent with expansion (Higdon 1996). In NGC 7714, the data are inconclusive on this point. The isovelocity contours do curve slightly when crossing the stellar ring (Figure 8a), and the gas is slightly blueshifted at the ring relative to circular motion, implying expansion, if one assumes the NGC 7714 tails are trailing. However, interpretation is complicated by the fact that large peculiar motions are seen in the nearby bridge, making it hard to separate possible radial or non-planar motions in the bridge from those in the ring. Also, the fact that the gas in the vicinity of the stellar ring is not confined to a ring-like structure makes interpretation of its motions uncertain. The isovelocity curves across the northwestern loop also do not show pronounced kinks, thus neither ring shows clear evidence for expansion. The fact that these are asymmetric rings likely caused by a very off-center encounter may also contribute to the lack of clearly defined velocity deviations at the rings.

Another possibility is that the stellar ring in this system is simply a wrapped-around spiral arm caused by a non-collisional prograde planar encounter, as in some of the models of Thomson & Wright (1990), Donner, Engström, & Sundelius (1991), Elmegreen et al. (1991), and Howard et al. (1993), rather than a collisional ring. The high column density of gas in the bridge, however, and its offset from the stars, supports the idea that gas was forced out of the main galaxy by a collision between two gas disks rather than merely perturbed in a grazing or long-range encounter. This possibility should be investigated further with hydrodynamical simulations of such encounters.

6. Conclusions

In this paper, we have presented both optical and 21 cm HI maps of the interacting pair NGC 7714/7715. This pair is connected by two bridges: a gaseous bridge, in which star formation is on-going, and a stellar bridge, which is parallel to but displaced 10" (1.8 kpc) to the south of the gaseous bridge. This offset persists 2'.7 (30 kpc) from the bridge through NGC 7715 and the countertail east of NGC 7715. In the main body of NGC 7714, there is no prominent HI counterpart to the stellar ring. Instead, we find a clumpy interstellar medium with maxima near the prominent star formation complexes in the disk, and a prominent HI loop on the opposite side of the galaxy. We also detect redshifted HI absorption towards the NGC 7714 nucleus, suggesting infall onto the starburst nucleus.

The velocity field of the inner disk of NGC 7714 shows the standard 'spider diagram' signature of an inclined rotating disk. At radii larger than 20" (3.5 kpc) pronounced deviations from circular motion are present, particularly at the bridge, indicating nonplanar and/or radial motions. Signs of rotation are also observed at NGC 7715. The gas in the immediate vicinity of NGC 7715 appears kinematically distinct from the gas in the surrounding extended structures.

We suggest that the peculiar morphology of this system is the result of a very off-center collision between two gas-rich disk galaxies. Our numerical simulations indicate that such collisions can create bridge/ring systems similar to NGC 7714/7715, in which the bridge contains both gas and stars. We conclude that the bridge in NGC 7714/7715 is a hybrid between classical tidal bridges, such as that in seen in M51, and gaseous 'splash' bridges observed in ring galaxies such as the Cartwheel. The observed offset between the gas and stars in this bridge may have been caused by dissipative collisions between gas clouds from the two galaxies. Further investigations of the interaction parameters for the NGC 7714/7715 encounter are needed to better define the roles of tidal 'swing' and collisional 'splash' in the NGC 7714/7715 bridge, and to better match the details of the system.

We would like to thank the staff at NRAO for their help in obtaining and reducing the data. In particular, James Higdon provided much assistance with the data reduction and many helpful comments. Data from the Digitized Sky Survey were used in this study. This research has made use of the NASA/IPAC Extragalactic Database (NED) which is operated by the Jet Propulsion Laboratory, California Institute of Technology, under contract with the National Aeronautics and Space Administration. This research was supported in part by NASA grant NAG 2-67. A portion of this work was performed while B.J.S. held a National Research Council Research Associateship at the Jet Propulsion Laboratory. R.W.P. was supported in part by NSF grant AST-9112879.

REFERENCES

Appleton, P. N., & Struck-Marcell, C. 1987, ApJ, 318, 103

Appleton, P. N., Charmandaris, V., & Struck, C. 1996, ApJ, 468, 532.

Arp, H. C. 1966, Atlas of Peculiar Galaxies, (Pasadena: California Institute of Technology)

Barnes, J. E., & Hernquist, L. 1991, ApJ, 370, L65

Begeman, K. G. 1989, A&A, 223, 47

Bernlöhr, K. 1993, A&A, 268, 25

Bowen, D. V., Osmer, S. J., Blades, J. C., Tytler, D., Cottrell, L., Fan, X.-M., & Lanzetta, K. M. 1994, AJ, 107, 461

Bushouse, H. A. 1987, ApJ, 320, 49

Bushouse, H. A., & Werner, M. W. 1990, ApJ, 359, 72

Clark, B. G. 1980, A&A, 89, 377

Condon, J. J., Helou, G., Sanders, D. B., & Soifer, B. T. 1990, ApJS, 73, 359

Condon, J. J., Helou, G., Sanders, D. B., & Soifer, B. T. 1993, AJ, 105, 1730

De Robertis, M. M., & Shaw, R. A. 1988, ApJ, 329, 629

de Vaucouleurs, G., de Vaucouleurs, A., Corwin, H. G., Jr., Buta, R. J., Paturel, G., & Fouque, P. 1991, Third Reference Catalogue of Bright Galaxies, (New York: Springer-Verlag) (RC3)

Dickey, J. M. 1986, ApJ, 300, 190

Donner, K. J., Engström, S., & Sundelius, B. 1991, A&A, 252, 571

Elmegreen, D. M., Sundin, M., Elmegreen, B., & Sundelius, B. 1991, A&A, 244, 52

Fosbury, R. A. E., & Hawarden, T. G. 1977, MNRAS, 178, 473

French, H. B. 1980, ApJ, 240, 41

Gerber, R. A., Lamb, S. A., & Balsara, D. S. 1992, ApJ, 399, L55

Gerber, R. A., Lamb, S. A., & Balsara, D. S. 1996, MNRAS, 278, 345

González-Delgado, R. M., Pérez, E., Días, Á. I., Garciá-Vargas, M. L., Terlevich, E., & Vilchez, J. M. 1995, ApJ, 439

Hernquist, L., & Weil, M. L. 1993, MNRAS, 261, 804

Hibbard, J. E., Guhathakurta, P., van Gorkom, J. H., & Schweizer, F. 1994, AJ, 107, 67

Hibbard, J. E., & van Gorkom, J. H. 1996, AJ, 111, 655.

Higdon, J. L. 1995, ApJ, 455, 524

Higdon, J. L. 1996, ApJ, 467, 241

Howard, S., Keel, W. C., Byrd, G., & Burkey, J. 1993, ApJ, 417, 502

Humason, M. L., Mayall, N. U., & Sandage, A. R. 1956, AJ, 61, 97

Ishizuki, S. 1993, Ph.D. Thesis, University of Tokyo

Keel, W. C. 1984, ApJ, 282, 75

Lynds, R., & Toomre, A. 1976, ApJ, 209, 382

Maloney, P., & Black, J. H. 1988, ApJ, 325, 389

Marcum, P. M., Appleton, P. N., & Higdon, J. L. 1992, ApJ, 399, 57

Marston, A. P., & Appleton, P. N. 1995, AJ, 109, 1002

Mihos, J. C., & Herquist, L. 1996, ApJ, 464, 641

Mirabel, I. F., & Sanders, D. B. 1988, ApJ, 335, 104

Neff, S. G., Hutchings, J. B., & Gower, A. C. 1989, AJ, 97, 1291

Peterson, S. D., & Shostak, G. S. 1974, AJ, 79, 767

Sanders, D. B., Scoville, N. Z., & Soifer, B. T. 1991, ApJ, 370, 158

Schweizer, F. 1978, in IAU Symposium 77, Structure and Properties of Nearby Galaxies, ed. E. M. Berkhuijsen and R. Wielebinski (Dordrecht: Reidel), p. 279

Smith, B. J., & Wallin, J. F. 1992, ApJ, 393, 544

Smith, B. J. 1994, AJ, 107, 1695

Smith, B. J. 1989, Ph.D. Dissertation, University of Massachusetts

Soifer, B. T., Sanders, D. B., Madore, B. F., Neugebauer, G., Danielson, G. E., Elias, J. H., Lonsdale, C. J., & Rice, W. L. 1987, ApJ, 320, 238

Struck-Marcell, C. 1990, AJ, 99, 71

Struck-Marcell, C., & Appleton, P. N. 1987, ApJ, 323, 480

Struck-Marcell, C., & Higdon, J. L. 1993, ApJ, 411, 108

Struck, C. 1996a, ApJ, submitted

Struck, C. 1996b, ApJ, submitted

Struck, C., Appleton, P. N., Borne, K. D., & Lucas, R. A. 1996, AJ, in press

Surace, J. A., Mazzarella, J., Soifer, B. T., & Wehrle, A. E. 1993, AJ, 105, 864

Theys, J. C., & Spiegel, E. A. 1977, ApJ, 212, 616

Thomson, R. C., & Wright, A. E. 1990, MNRAS, 247, 122

Toomre, A., & Toomre, J. 1972, ApJ, 178, 623

van Breugel, W., Filippenko, A. V., Heckman, T. M., & Miley, G. K. 1985, ApJ, 293, 83

van Gorkom, J. H., Knapp, G. R., Ekers, R. D., Ekers, D. D., Laing, R. A., & Polk, K. S. 1989, AJ, 97, 708

Wallin, J. F., & Struck-Marcell, C. 1994, ApJ, 433, 631

Weedman, D. W., Feldman, F. R., Balzano, V. A., Ramsey, L. W., Sramek, R. A., & Wu, C.-C. 1981, ApJ, 248, 105

Wever, B. M. H. R., Appleton, P. N., Davies, R. D., & Hart, L. 1984, A&A, 140, 125

Wright, A. E. 1972, MNRAS, 157, 309

Young, J. S., & Devereux, N. A. 1991, ApJ, 373, 414

This manuscript was prepared with the AAS $\mbox{\sc IAT}_{\mbox{\sc E}}\mbox{\sc X}$ macros v4.0.

Captions

Figure 1. The B+C+D Array channel maps for NGC 7714/7715. The beamsize is $11''.02 \times 8''.48$ with a position angle of $-36^{\circ}.6$ and the noise level is 0.3 mJy beam⁻¹. The first contour is 1.28 mJy beam⁻¹; the contour interval is 2.56 mJy beam⁻¹. The crosses indicate the locations of the nuclei of the two galaxies.

Figure 2. (a) The narrowband red continuum ($\lambda = 6560 \text{Å}$; $\Delta \lambda = 50 \text{Å}$) image of the NGC 7714/7715 system. NGC 7715 lies to the east of NGC 7714. The contours are logarithmically spaced, with $\Delta \log(F) = 0.12$. These data have been smoothed to 3" resolution for clarity. The brightening in the lower left corner of this figure is due to a very bright star near the edge of the image. (b) The H α image of the NGC 7714/7715 system. NGC 7714 and the HII regions in the bridge are visible in this image. NGC 7715 is not seen in this image because it does not have on-going star formation. The first contour is $3.9 \times 10^{-16} \text{ erg s}^{-1} \text{ cm}^{-2} (3\sigma)$. The contour interval is logarithmic, with $\Delta \log(F) = 0.5$. The features outside of NGC 7714 and the bridge are artifacts caused by imperfect stellar subtraction.

Figure 3. The B Array 20 cm continuum map. The beamsize is $6''.32 \times 5''.79$ with a positions angle of 2°.7, while the rms noise level is 0.18 mJy/beam. The first contour level is 0.72 mJy/beam. The contour interval is logarithmic, with $\Delta \log(F) = 0.5$.

Figure 4. (a) The naturally-weighted B Array HI intensity map. The spatial resolution is $6''.32 \times 5''.78$. The first contour level and the contour interval are 4×10^{20} cm⁻². (b) The naturally-weighted B+C+D Array HI intensity map. The beamsize is $11''.02 \times 8''.48$ with a position angle of $-36^{\circ}.6$. The first contour level is 2×10^{20} cm⁻² and the contour interval is 4×10^{20} cm⁻².

Figure 5. (a) The B Array HI intensity map (greyscale) $(6''.32 \times 5''.78 \text{ beam})$, superposed

on the narrowband red continuum image (contours). (b) The B Array HI intensity map (greyscale) (6".32 \times 5".78 beam), superposed on the H α contours.

Figure 6. The POSS-I red image, smoothed to 12" resolution (contours), superposed on the B+C+D Array HI intensity map (greyscale). A bright star in the lower left corner of the optical image causes a background gradient across the image.

Figure 7. HI spectra for the various structures in the NGC 7714/7715 system, as in Table 3. Note that the NGC 7715 spectrum has been scaled up by a factor of four.

Figure 8. (a) The B+C+D Array velocity field (contours), superposed on the red continuum image (greyscale). The contour interval is 10 km s⁻¹. Several contours are labeled. (b) The velocity field (contours), superposed on the B+C+D Array HI intensity map (greyscale). The contour interval is 10 km s⁻¹. Several contours are labeled.

Figure 9. The rotation curve for NGC 7714. This was derived assuming a constant inclination of 30° , a systemic velocity of 2800 km s^{-1} , and a line of nodes of 136° east of north.

Figure 10. The continuum-subtracted HI spectrum for the nucleus of NGC 7714, from the B Array data.

Figure 11. A numerical simulation of an off-center collision between two unequal mass disk galaxies (see text), at a time 10⁸ yrs after the point of closest approach. This model was run with a smooth particle hydrodynamics code as described in the text. Panel a shows an x-y view of the distribution of stars. In panels b and c, the distribution of gas in the x-y and x-z planes, respectively, are displayed. Panel d gives an expanded x-y view of both the gas and stars in the bridge. In panels a-c, every 10th gas particle and every 3rd star particle are plotted. In panel d, every 5th gas particle and every 2nd star are plotted, and the stars are plotted as plus signs.

 ${\bf Table~1}$ Basic Information on the NGC 7714/7715 System

Galaxy	NGC 7714	NGC 7715	Notes
$\alpha(1950)$	$23^{\rm h}33^{\rm m}40.6$	$23^{\rm h}33^{\rm m}48.3$	a
$\delta(1950)$	1°52′42″	1°52′48″	a
Type	SBb Pec	Irr Pec	b
B_T	13.0	14.7	b
Velocity	$2808 \pm 15 \; \mathrm{km \; s^{-1}}$	$2812 \pm 31 \; \mathrm{km \; s^{-1}}$	c

^aFor NGC 7714, radio continuum position from Condon et al. 1990. For NGC 7715, optical position measured with the Grant machine at N.O.A.O. (Smith 1989).

 $^{^{}b}$ de Vaucouleurs et al. 1991.

 $[^]c{\rm Optical}$ velocities tabulated in de Vaucouleurs et al. 1991.

 ${\bf Table~2}$ Background 20 cm Continuum Sources in the NGC 7714 field

Source		R.A.			Dec		Peak F_{20}^{a}
		(1950))		(1950))	(mJy)
#1	23 ^h	33 ^m	57°.54	1°	54'	16"	30.5
#2	$23^{\rm h}$	33^{m}	57°.14	1°	54'	8"	42.7
#3	$23^{\rm h}$	33^{m}	$56^{\rm s}\!.34$	1°	53'	56"	54.8

 $[^]a {\rm In}$ the 6″.32 \times 5″.79 naturally-weighted B Array beam.

 ${\bf Table~3}$ HI Structures in the NGC 7714/7715 System a

Source	$R.A.^b$		$\mathrm{Dec.}^b$		b	$Velocity^c$	$\Delta \mathbf{V}^d$	${ m M}_{HI}$	peak $N(HI)^e$	
	(1950)		(1950)		0)	$({\rm km~s^{-1}})$	$({\rm km~s^{-1}})$	$({\rm M}_{\odot})$	(cm^{-2})	
Eastern Cloud	23	33	51.1	1	53	12	2750	40	3.8×10^{8}	1.8×10^{21}
Bridge	23	33	44.9	1	52	50	2790	50	1.5×10^9	4.2×10^{21}
Northwestern Loop	23	33	42.7	1	53	32	2880	120	1.1×10^9	1.7×10^{21}
Southwestern Clump	23	33	39.5	1	52	28	2820	70	2.9×10^8	4.1×10^{21}
Northwestern Clump	23	33	40.7	1	52	52	2850	80	2.4×10^8	3.8×10^{21}
Southeastern Arc	23	33	40.9	1	52	24	2760	60	2.1×10^8	2.8×10^{21}
Total System	23	33	44.9	1	52	50	2800	140	7.0×10^9	4.2×10^{21}
NGC 7714^f	23	33	39.5	1	52	28	2830	150	1.7×10^9	4.1×10^{21}
NGC 7715^g	23	33	49.1	1	52	58	2760	80	3.1×10^8	1.9×10^{21}

 $[^]a\mathrm{All}$ results from the B+C+D Array data.

 $^{{}^}b\mathrm{Position}$ of peak HI column density.

 $[^]c\mathrm{Peak}$ velocity.

 $[^]d$ Full Width Half Maximum.

 $[^]e \text{In a } 11\rlap.{''}02 \times 8\rlap.{''}48$ beam.

 $[^]f For a 50'' \times 50''$ region centered on the NGC 7714 nucleus. Includes the two clumps and the southeastern arc listed above.

 $[^]g \text{For a } 30^{\prime\prime} \times 30^{\prime\prime} \text{ region centered on the NGC 7715 nucleus.}$

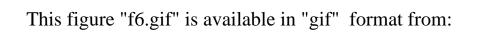
This figure "f1.gif" is available in "gif" format from:

This figure "f2.gif" is available in "gif" format from:

This figure "f3.gif" is available in "gif" format from:

This figure "f4.gif" is available in "gif" format from:

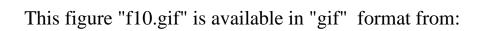
This figure "f5.gif" is available in "gif" format from:



This figure "f7.gif" is available in "gif" format from:



This figure "f9.gif" is available in "gif" format from:



This figure "f11.gif" is available in "gif" format from: